NACE INTERNATIONAL

CORROSION
Conference & Expo
2019

Fundamental Mechanisms of Mild Steel Corrosion in H_2S Containing Environments

Aria Kahyarian, Bruce Brown, Srdjan Nesic
Institute for Corrosion and Multiphase Flow Technology, Ohio University
342 W. State St.
Athens, Ohio, 45701
USA

ABSTRACT

The current understanding of the corrosion mechanisms in H_2S containing environments is based on the direct electrochemical reduction of H_2S as the main contribution of this species to the corrosion process. Such an argument has been developed based on the distinctive behavior of cathodic polarization curves in H_2S containing solutions, as compared to the behavior observed in the solutions of strong acids or those in presence of other weak acids such as carboxylic acids and carbonic acid. The direct reduction of H_2S is generally associated with the observation of a "double wave" in a cathodic polarization curve. In the present study, the mechanism of cathodic reaction in H_2S containing acidic solutions was studied theoretically with the aid of a comprehensive mathematical model. The model includes a mechanistic description of main processes including mass transfer, chemical reactions, and electrochemical reactions. A quantitative analysis based on this model showed that all the characteristic behaviors previously associated with the direct reduction of H_2S, including the "double wave" behavior, can be explained based on the kinetics of homogeneous chemical dissociation of H_2S and hydrogen ion reduction as the sole cathodic reaction. This analysis suggests that H_2S is not a significant electroactive species, and its main contribution to the corrosion process is through its buffering ability as a weak acid, similar to other weak acids such as carboxylic acids and carbonic acid. In order to validate these mechanistic observations, the results from this model were compared to existing experimental data from the open literature. The model was found to be able to capture the main characteristic experimental behavior with reasonable accuracy, further supporting this mechanistic argument.

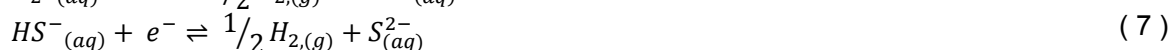Key words: Hydrogen sulfide, Corrosion, Mechanism, Mild steel, Electrochemical, Polarization

INTRODUCTION

In the presence of an aqueous medium, the hydrogen sulfide (H_2S) in the gas phase can dissolve and dissociate according to equilibrium Reactions (1) to (3). As a weak acid, H_2S is only partially dissociated

in the aqueous phase leading to a chemical equilibria. The presence of these sulfide species in the solution has been observed to dramatically influence the corrosion process, both in terms of their electrochemical tendencies [1–7] and perhaps more importantly, due to their contribution in formation of a corrosion product layer [8–10].

$$H_2S_{(g)} \rightleftharpoons H_2S_{(aq)} \qquad (1)$$
$$H_2S_{(aq)} \rightleftharpoons HS^-_{(aq)} + H^+_{(aq)} \qquad (2)$$
$$HS^-_{(aq)} \rightleftharpoons S^{2-}_{(aq)} + H^+_{(aq)} \qquad (3)$$

The present study is focused on the basic mechanisms of the H_2S contribution to the cathodic currents during the corrosion process. The acidic corrosion of steel in the presence of H_2S is believed to be the result of electrochemical dissolution of iron (anodic partial of Reaction (4)) as the main anodic reaction, accompanied by a series of cathodic hydrogen evolving reactions as shown via the cathodic partials of Reactions (5) to (8). These include the hydrogen ion (H^+) and water (H_2O) reduction (Reactions (5) and (8), respectively), which are well-known processes in metallic corrosion in de-aerated aqueous acidic systems. Furthermore, in the context of H_2S corrosion, the direct reduction of H_2S and HS^- (Reactions (6) and (7), respectively) are commonly presumed to contribute to cathodic currents[3,11–14,5,15,7,6,2].

$$Fe^{2+} + 2e^- \rightleftharpoons Fe \qquad (4)$$
$$H^+_{(aq)} + e^- \rightleftharpoons {}^1\!/_2\, H_{2,(g)} \qquad (5)$$
$$H_2S_{(aq)} + e^- \rightleftharpoons {}^1\!/_2\, H_{2,(g)} + HS^-_{(aq)} \qquad (6)$$
$$HS^-_{(aq)} + e^- \rightleftharpoons {}^1\!/_2\, H_{2,(g)} + S^{2-}_{(aq)} \qquad (7)$$
$$H_2O_{(aq)} + e^- \rightleftharpoons {}^1\!/_2\, H_{2,(g)} + OH^-_{(aq)} \qquad (8)$$

The assumptions about the electrochemical contribution of H_2S to the cathodic currents can be found in studies as early as 1965, reported by Bolmer[3]. The direct H_2S reduction reaction was also assumed to contribute to the observed polarization cathodic currents obtained in rotating disk experiments by Morris et al.[11]. The proposed electrochemical activity of the H_2S became an accepted mechanism of corrosion in H_2S system in the subsequent studies [12–14,5,15]. Nevertheless, a systematic investigation of this mechanistic aspect was not done until more recent years. In 2013, Kittel et al. investigated the cathodic polarization curves of a H_2S containing solution on a stainless steel surface [7]. The previous reports of the significant effect of H_2S on the limiting current was confirmed in that study. Furthermore, the authors showed that in certain conditions a "double wave" shape appears in the polarization curves; an observation that was considered as solid proof for the direct H_2S reduction reaction. The observed double wave was associated with the existence of two electrochemical reactions and their corresponding limiting currents, one being the H^+ reduction and other being the H_2S reduction reaction. The experimental findings of this study were further used to developed a mathematical model of the cathodic polarization behavior in H_2S containing solutions [6]. The model proposed in that study included both the H^+ and H_2S cathodic reactions and also the homogeneous chemical reactions associated with the H_2S/H_2O system.

In a paralel study[2], Zheng et al. investigated the mechanism of the mild steel corrosion in the presence of H_2S, using a wider range of experimental conditions. The effect of H_2S on the limiting current, and the existence of two limiting currents (i.e. the "double wave") was also reported in that study. The authors noted that both limiting currents, associated with the H^+ and H_2S reduction reactions, were the result of mass transfer limitation of the involved reactants. These observations led the authors to conclude that in H_2S containing solutions, the direct reduction of H_2S is a significant cathodic process. Zheng et al. also developed an elementary mechanistic model [16] based on these findings, where a reasonable agreement with the experimental data was reported. In 2017, Esmaeely et al. reported a set of experimental polarization data at pH_2S of 1 bar [4] on a mild steel surface. The reported polarization curves were found to behave similarly to those obtained at lower H_2S partial pressures in earlier studies [2,17]. The authors used a similar model to that proposed by Zheng et al. [2] to quantify their experimental data.

In the present study, the effect of homogeneous dissociation of H_2S inside the diffusion boundary layer on the polarization response of the system was investigated in more depth. For that purpose, a comprehensive mathematical model was developed in order to incorporate the effect of the homogeneous reactions and the transport processes on the surface concentration of H^+. As discussed further in the following sections, the results show that the buffering effect of H_2S is indeed significant in nearly all typical conditions. The increased limiting currents and the observed "double wave" are readily explained by the homogeneous H_2S dissociation reaction, without considering the direct reduction of H_2S. The simulated polarization curves are also compared to the recent experimental data reported in the literature, and a reasonable agreement was found.

THE MATHEMATICAL MODEL

The mathematical model used in the present discussion is similar to those described in detail in our previous studies [16,18,19]. The model consists of a water chemistry calculations module to obtain solution speciation at the bulk. The governing transport of species is defined by the Nernst-Planck equation, which describes the concentration distribution of various species through the diffusion layer, as discussed below. Finally, the boundary condition at the metal/solution interface incorporates the electrochemical nature of the corrosion process into the model and is defined based on the rate of the underlying electrochemical reactions.

Water chemistry

Upon dissolution in water, the dissolved H_2S, as a diprotic weak acid, is partially dissociated to form HS^-, S^{2-} and H^+. This reaction sequence is described according to the chemical Reactions (1) to (3), above. In an aqueous solution the dissociation of water, as the solvent, also occurs as shown by Reaction (9).

$$H_2O_{(l)} \rightleftharpoons OH^-_{(aq)} + H^+_{(aq)} \qquad (9)$$

The dissolution of H_2S in water (equilibrium Reaction (1)) can be described according to Henry's law, assuming ideal conditions, where $C_{H_2S_{(aq)}}$ (M) is the concentration of the dissolved H_2S, $p_{H_2S_{(g)}}$ is the partial pressure of H_2S (bar), and H_{H_2S} is the Henry's constant, as shown in Table 1.

$$\frac{C_{H_2S_{(aq)}}}{p_{H_2S_{(g)}}} = H_{H_2S} \qquad (10)$$

The chemical equilibria of the dissociation Reactions (2) and (3) can be expressed mathematically via Equations (11) and (12), with K_{H_2S} and K_{HS^-} being the equilibrium constants of the H_2S and HS^- dissociation reactions, respectively, as shown in Table 1.

$$\frac{C_{HS^-_{(aq)}} C_{H^+_{(aq)}}}{C_{H_2S_{(aq)}}} = K_{H_2S} \qquad (11)$$

$$\frac{C_{S^{2-}_{(aq)}} C_{H^+_{(aq)}}}{C_{HS^-_{(aq)}}} = K_{HS^-} \qquad (12)$$

The water dissociation reaction, ionic product of K_w (see Table 1), can also be expressed as:

$$C_{OH^-_{(aq)}} C_{H^+_{(aq)}} = K_w \qquad (13)$$

Table 1. Physiochemical constants of the H_2S/H_2O system at 25 °C.

Parameter	Value	Units	Reference
K_w	9.84×10^{-15}	(M^2)	[20]
H_{H_2S}	9.71×10^{-2}	$(M.bar^{-1})$	[21]
K_{H_2S}	1.04×10^{-7}	(M)	[22]
K_{HS^-}	5.75×10^{-18}	(M)	[23]
k_{b,H_2S}	7.5×10^{10}	$(M^{-1}.s^{-1})$	[24]
k_{b,HS^-}	8×10^{10}	$(M^{-1}.s^{-1})$	Estimated
$k_{b,w}$	1.4×10^{11}	$(M^{-1}.s^{-1})$	[25,26]
D_{H_2S}	1.93×10^{-9}	$(m^2.s^{-1})$	[27]
D_{HS^-}	1.73×10^{-9}	$(m^2.s^{-1})$	[28]
$D_{S^{2-}}$	1.5×10^{-9}	$(m^2.s^{-1})$	Estimated
D_{H^+}	9.31×10^{-9}	$(m^2.s^{-1})$	[29]
D_{OH^-}	5.27×10^{-9}	$(m^2.s^{-1})$	[28]
D_{Na^+}	1.33×10^{-9}	$(m^2.s^{-1})$	[29]
D_{Cl^-}	2.03×10^{-9}	$(m^2.s^{-1})$	[28,29]

In addition to the equilibrium relationships, the solution speciation has to satisfy the electro-neutrality constraint, shown as Equation (14).

$$\sum_i z_i C_i = 0 \tag{14}$$

At a known solution pH and partial pressure of H_2S, the solution speciation can be readily calculated based on Equations (10) to (13) and the electro-neutrality constraint shown as Equation (14). Figure 1 demonstrates the results of such calculations for an open system at 0.1 and 1 bar H_2S partial pressures for a range of pH values.
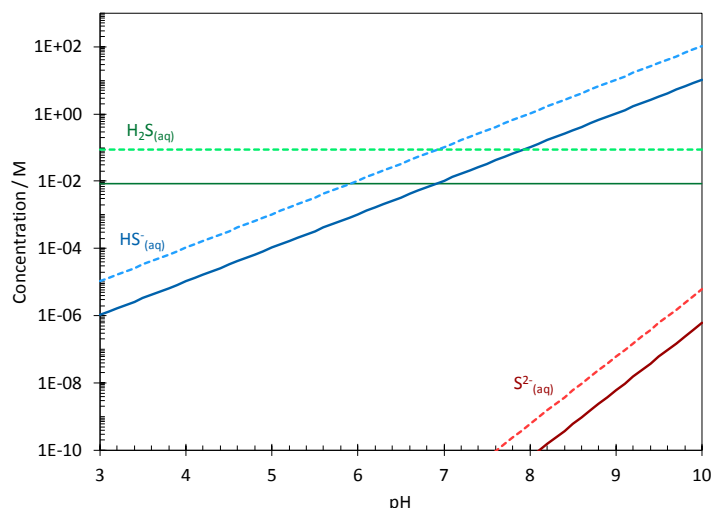
Figure 1. The calculated solution speciation of H₂S/H₂O system at 25°C, for 0.1 bar H₂S (solid lines), and 1 bar H₂S (dashed lines).

Governing equations

Considering the heterogeneous nature of the electrochemical reactions, their rates are defined based on the surface concentration of the active species, which are not known explicitly. However, these concentrations can be calculated based on the Nernst-Planck Equation (15), when the appropriate initial and boundary conditions are used.

$$\frac{\partial C_i}{\partial t} = -\nabla . N_i + R_i \tag{15}$$

Equation (15) describes the concentration distribution of species i, where N_i is the flux, and R_i is the source term that includes the consumption/production of species i through homogeneous chemical reactions. The flux of any given species can be described through Equation (16) [29], where the terms on the right hand side, describe the effect of electro-migration, molecular diffusion, and convective flow, respectively.

$$N_i = -z_i u_i F C_i \nabla \phi - D_i \nabla C_i + v C_i \tag{16}$$

Considering the symmetry of the electrode, the tangential and radial species flux components of Equation (15) and Equation (16) can be neglected. Furthermore, the mobility of ions can be estimated using Nernst-Einstein relationship ($u_i=D_i/RT$), with the diffusion coefficients listed in Table 1. Hence, the equations above can be simplified to Equation (17) and Equation (18):

$$N_i = -D_i \frac{\partial C_i}{\partial x} - \frac{z_i D_i F C_i}{RT} \frac{\partial \phi}{\partial x} + v_x C_i \tag{17}$$

$$\frac{\partial C_i}{\partial t} = D_i \frac{\partial}{\partial x} \frac{\partial C_i}{\partial x} + \frac{\partial}{\partial x} \left(\frac{z_i D_i F C_i}{RT} \frac{\partial \phi}{\partial x} \right) - v_x \frac{\partial C_i}{\partial x} + R_i \tag{18}$$

In the convective term, v_x describes the velocity profile inside the diffusion layer. For example, for the case of a rotating disk electrode (RDE), the analytical solutions for the velocity profile (v_x) and the diffusion layer thickness (δ) are shown as Equation (19), where a = 0.510, and Equation (20), respectively [30].

$$v_x = -a\omega \left(\frac{\omega}{v}\right)^{1/2} x^2 \qquad (19)$$

$$\delta = \left(\frac{3D_{lim}}{av}\right)^{1/3} \left(\frac{\omega}{v}\right)^{-1/2} \qquad (20)$$

As mentioned above, the rate of consumption/production of the chemical species via the homogeneous chemical reactions are incorporated in these calculations through the R_i term in Equation (18). The rate of chemical reaction j, presented in the form of Reaction (21) is expressed as Equation (22).

$$\sum_{r=1}^{n_r} C_r \rightleftharpoons \sum_{p=1}^{n_p} C_p \qquad (21)$$

$$R_j = k_{f,j} \prod_{r=1}^{n_r} C_r - k_{b,j} \prod_{p=1}^{n_p} C_p \qquad (22)$$

where $k_{f,j}$ and $k_{b,j}$ are the reaction rate constants of the forward and backward reactions. Here, the solution inside the diffusion boundary layer is treated as a single aqueous phase. The relevant chemical reactions are therefore, the dissociation of H_2S, HS^-, and H_2O. The kinetic rate constants for these reactions can be found in Table 1. For each chemical species i, R_i is the sum of the rates corresponding to all j chemical reactions involving this species, as shown in Equation (23).

$$R_i = \sum_j R_j \, s_{i,j} \qquad (23)$$

In Equation (23), the rate of reaction where species i is produced is expressed as a positive value, and when it is consumed as a negative value, and $s_{i,j}$ is the stoichiometric coefficient of species i in reaction j. In addition to the concentration of species, the potential of the solution inside the diffusion boundary layer has to be specified in order to calculate the effect of electro-migration, as seen in Equation (18). This parameter can be obtained by using an additional relationship known as "electro-neutrality" constraint, which was already introduced as Equation (14).

Initial and boundary conditions

As a second order partial differential equation, Equation (18) can only be solved if the appropriate boundary and initial conditions are specified. At the initial time ($t = 0$), it can be assumed that a well-mixed solution comes into contact with the metal surface. Hence, the concentrations of the chemical species throughout the diffusion layer are constant known values, defined by the chemical equilibria of the solution as obtained from the water chemistry calculations. Furthermore, at the bulk solution boundary, where $x = \delta$, the concentration of chemical species remains unchanged at all times ($t \geq 0$).

The boundary condition at the metal/solution interface can be specified in term of the flux of the chemical species as defined by electrochemical reactions. For an electroactive chemical species, the flux at the metal/solution interface is equal to the rate of its consumption/production through the heterogeneous electrochemical reactions. Therefore, for species i involved an electrochemical reaction, it can be stated that:

$$N_i|_{x=0} = -\frac{s_i i}{nF} \qquad (24)$$

The negative sign in Equation (24) is due to a sign convention where the cathodic current is taken as negative. Furthermore, for the reaction written in "cathodic" form (e.g. Reaction (5)), the reactants on

the left hand side are represented with a negative stoichiometric coefficient (s_{ij}) and the product on the right hand side is represented with a positive value.

The present study is focused on the cathodic current in the potential range close to the corrosion potential. Therefore, the anodic iron dissolution and water reduction reactions are not included in the present discussion. Additionally, the present study attempts to investigate if the polarization curves can be explained without considering the direct reduction of sulfide species (Reactions (6) and (7)). Therefore, the only electrochemical reaction in the present model is the one describing the H^+ reduction. Due to the negligible concentration of H_2 in the solution, no significant contribution of the hydrogen oxidation reaction in the potential range of interest is expected. Hence, the cathodic current density resulting from hydrogen ion reduction was calculated in the form shown in Equation (25). The kinetic parameters, including transfer coefficient $\alpha_{H^+} = 0.5$, the reaction rate constant $k_{0_{H^+}} = 1.2E - 8$, and the reaction order $m_{H^+} = 0.5$, used in this model, were estimated based on the experimental data previously reported in the literature, as discussed in the following section.

$$i_{c,H^+} = -n_{H^+} F k_{0_{H^+}} C_{H^+}^{S \, m_{H^+}} e^{\left(\frac{-\alpha_H + n_{H^+} F (E_{app} - E_{0_{H^+}})}{RT}\right)} \tag{25}$$

For non-electroactive species, the flux at the metal surface is zero, as it is a non-porous non-reactive barrier for these species:

$$N_i|_{x=0} = 0 \tag{26}$$

The flux Equations (25) and (26) can be used to describe the boundary conditions for all chemical species at the metal surface. Considering that the N_i appears in these relationships, the solution potential should also be specified at the solution/metal boundary. This can be done similar to that in the governing equations, using the electro-neutrality constraint as described by Equation (14).

Numerical Solution

Mathematical relationships described above are the main elements required to construct a comprehensive mathematical model for H_2S corrosion of mild steel. These equations form a set of non-linear, coupled, partial differential equations. Considering a simple one-dimensional spatial computational space, the finite difference method can be used to discretize them and solve the resulting algebraic equations numerically. This method is commonplace in mathematical modeling of electrochemical systems with similar geometry and has been discussed in detail elsewhere [16,18,29].

The partial differential equations are discretized using second order Taylor's series approximations. The time integration is done explicitly, using Euler approximation. The resulting algebraic equations can be written in a matrix format, as a tri-diagonal coefficient matrix multiplied by the unknown concentrations and solution potential. The final solution can then be obtained through different solution algorithms such as Neman's "BAND" open-source code where it is solved by LU decomposition method [29]. The presence of nonlinear terms, such as those in the electro-migration or chemical reactions relationships, makes some of the terms in the coefficient matrix a function of other concentrations and/or potential, i.e. they are not explicitly known. In the approach used in the present model, the final solution was obtained iteratively by using an initial guess for the unknown terms of the coefficient matrix (usually the last calculated value of the unknown term) until the desired accuracy was achieved.

<div align="center">
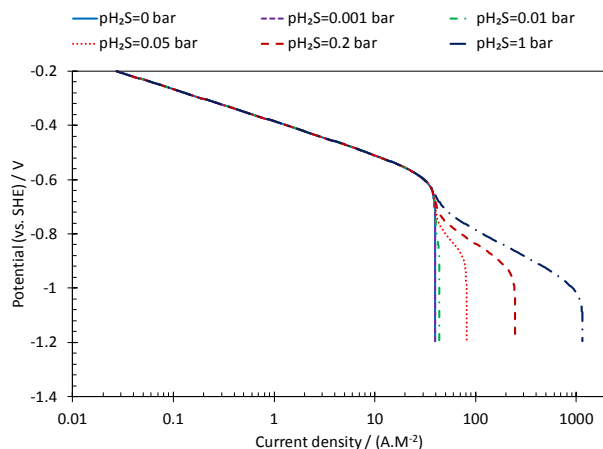
RESULTS

</div>

Theoretical discussion

Let us first entertain the idea that the buffering effect of H_2S can become significant at favorable environmental conditions. This is expected from any weak acid, including H_2S, as a result of their partial

dissociation in an aqueous environment. As shown in the water chemistry calculations, the extent of dissociation is a pH dependent phenomenon. Considering the recent findings in similar systems, weak acids with relatively low pKa (about 4), such as acetic acid, and carbonic acid, are strong buffers [18,31–33]. Meaning that their equilibrium and kinetic properties allow them to readily dissociate as the surface pH under mass transfer limitation is increased. In terms of reaction kinetics, the association of H_2S is categorized as "diffusion controlled", similar to association of water, carbonic acid, and acetic acid [24]. In this case, the term "diffusion controlled" refers to reactions with extreme rates that occur as soon as the reactants "collide" [24,34,35]. With pKa of about 7, H_2S appears to be thermodynamically and kinetically capable to exhibit, at least partially, the same buffering abilities.
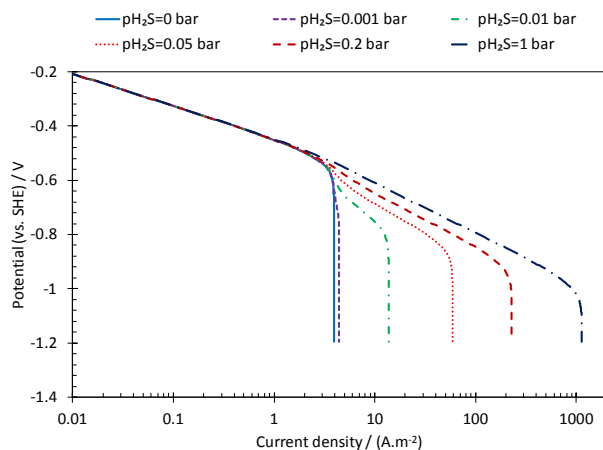
The theoretical significance of the buffering ability of H_2S is first discussed in terms of the simulated cathodic polarization curves, using the mathematical model developed above. As described, in this model H^+ reduction is the only cathodic reaction considered. Figure 2 demonstrates the predicted steady state polarization curves at the pH range from 3 to 5 and pH_2S of 0 to 1 bar. The results clearly demonstrate that the buffering effect of H_2S is indeed significant at almost all conditions, which results in a significant increase in the observed cathodic currents with increasing pH_2S. Furthermore, the characteristic cathodic "double wave", which was previously associated with its direct reduction [7,6,2,4,17] is successfully predicted in these voltammograms. As it is observed in Figure 2, the first limiting current can be associated with the mass transfer limitation of H^+ reduction, which is not affected by pH_2S, and remains constant at a constant pH. The second limiting current is due to the presence of H_2S in the solution. As the pH is increased, the potential at which this second wave is observed shifts towards more positive potentials. Also, the pH_2S at which the second wave appears decreases with increasing pH values. On the other hand, the characteristic double wave shape rapidly diminishes at higher pH values. Considering that the predicted results are solely based on H^+ reduction, these characteristic behaviors are all associated with the relative dominance of two processes that supply the H^+ at the electrode surface: the mass transfer of H^+ from the bulk solution, and the dissociation of H_2S at the vicinity of the metal surface.

In order to further analyze the nature of the observed double wave, the calculated surface chemistry during the polarization was studied. Figure 3 illustrates the current response of the simulation at pH 3 and pH_2S of 0.2 bar on the secondary axis, versus the calculated surface pH on the horizontal axis. The behavior of the surface concentration of H_2S and HS^- are shown in the same graph, on the primary vertical axis. As it appears in Figure 3, up to the current density of about 10 $A.m^{-2}$, the surface pH remains practically unchanged, which corresponds to the charge transfer controlled cathodic range observed in Figure 2.A. In this range, the surface concentration of all species is the same as that in the bulk solution. As the first limiting current density at about 40 $A.m^{-2}$ is reached, the surface pH starts to increase, as expected from a mass transfer limiting scenario. In this range, although the current density does not increase, the surface pH increases as the potential (the driving force of the reaction) decreased to more negative values. Ultimately, at a negative enough potential, the surface pH reaches a sufficiently high value that favors the dissociation of H_2S. This reaction becomes significant at surface pH values of about 5 and reaches its maximum at about pH 9. The crossing pH of H_2S and HS^- concentration trends occurs almost at the pKa value of H_2S. Considering the higher pKa of HS^- (about 17), no significant contribution from this reaction is expected in the surface pH range encountered at these conditions.
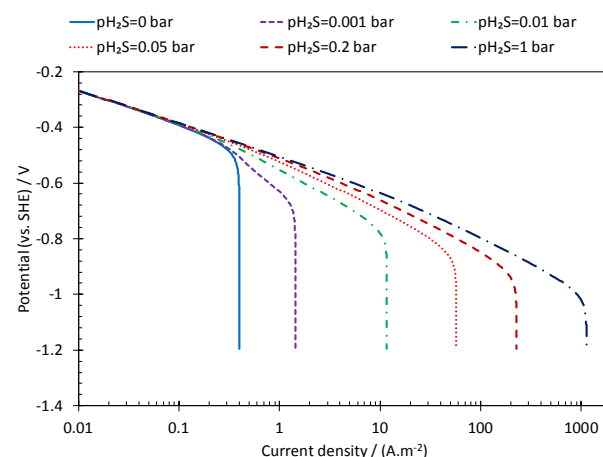
A)

B)

C)

Figure 2. Simulated steady state cathodic polarization behavior of acidic solutions containing H₂S, at 25ºC, 0.1 M NaCl, 2000 rpm RDE. A) pH 3. B) pH 4. C) pH 5.

As rule of thumb, when the mass transfer limited current of H⁺ reduction starts to appear, the surface pH is about 1-2 units higher than the bulk pH. Considering the case of a bulk pH of 5, that suggests the surface pH rapidly reaches the range that favors H₂S dissociation. That is the reason why a double wave is not clearly observed in this condition, as shown in Figure 2.C. On the other hand, at a bulk pH of 3, the surface pH favorable for H₂S dissociation is only reached at potentials substantially into the H⁺ reduction limiting current range; thus, the double wave is observed in an extended pH₂S range of Figure 2.A.
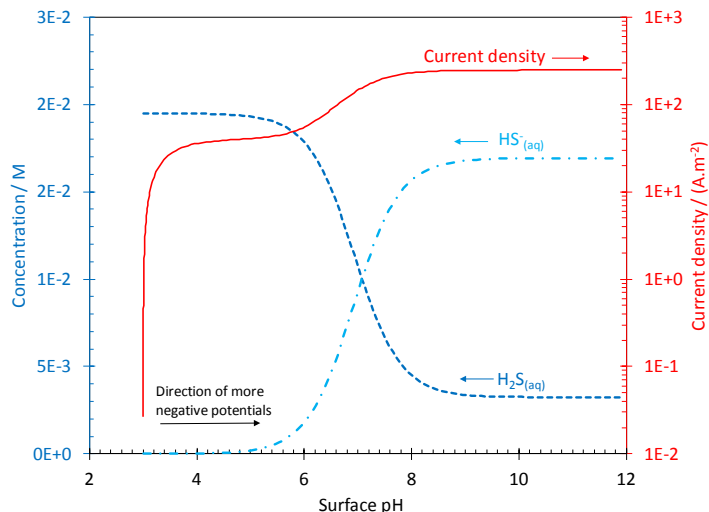
Figure 3. The relationship between the calculated surface pH and the surface concentration of H₂S and HS⁻, on the primary vertical axis, and the calculated current density, on the secondary vertical axis. Conditions: 25°C, 2000 rpm RDE, pH 3, pH₂S=0.2 bar, and the potential range from -0.2 to -1.2 V vs. SHE.

Experimental verification

In order to examine the validity of the above mechanistic observations further, the results obtained from this model were compared with the experimental data reported in the literature. The experimental polarization curve data of the present discussion was taken from a study by Zheng et al.[2]. The experiments in that study were done using rotating cylinder electrodes. In order to properly estimate the mass transfer effect, the equivalent rotation speed of a rotating disk electrode was obtained by equating the mass transfer coefficient from the two well-known Eisenberg [36] and Levich equations. The equivalent rotation speed (rpm) was obtained as:

$$\Omega_{RDE} = (0.0785 \times \Omega_{RCE}^{0.7} \, d_{RCE}^{0.4} \, v^{-0.177} \, D^{0.023})^2 \tag{27}$$

In the study by Zheng et al., the authors developed a mechanistic model of H₂S corrosion[2], where both H⁺ and H₂S were considered to be reduced at the metal surface. The comparison of the present model of cathodic current, solely based on H⁺ reduction and the buffering effect of H₂S, with the experimental data of Zheng et al. [2] is shown in Figure 4. A reasonable agreement with the experimental data was found, where the model was able to predict the main characteristic features of the cathodic polarization curves. Even though the present model does not include the direct reduction of H₂S, the simulated cathodic polarization curves were found to be at the same level of agreement with the experimental data, as those reported in the original study [2].
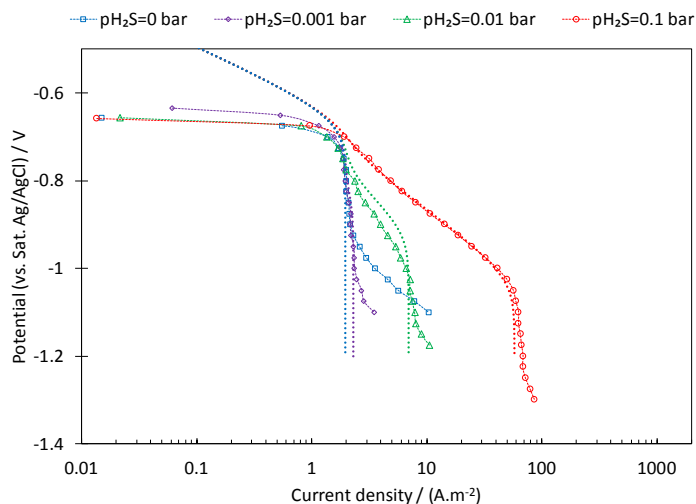
Figure 4. Cathodic polarization curves at pH 4, 30°C, 1000 rpm RCE (405 rpm RDE equivalent), at various H₂S partial pressures. The dotted lines show the results from the present model. The experimental data was taken from Zheng et al.[2].

The comparison of the results of the present model with the experimental cathodic polarization data reported by Zheng et al. at pH 4 and H₂S partial pressures up to 0.1 bar [2], show a good agreement in the limiting current densities. The presence of the double wave, and its position was also reasonably predicted by the model. It is worthwhile to notice that the current densities in between the two limiting currents show a clear dependence on the pH₂S. Nonetheless, they are properly estimated by the model solely based on H$^+$ reduction. This can be understood, considering the fact that the surface concentration of H$^+$ at this range is defined by the H₂S dissociation reaction. Naturally, the increased concentration of this species results in an increased rate of dissociation and hence, higher concentration of H$^+$ at the surface.

CONCLUSIONS

The theoretical analysis of the buffering effect of H₂S showed that at the typical conditions considered previously in the literature, the direct reduction of H₂S is not significant, similar to the case of acetic acid and carbonic acid. The increased limiting currents and the observed "double wave" behavior can be fully explained by the homogeneous dissociation of H₂S inside the diffusion boundary layer. It is shown that the buffering effect of H₂S is only observed when the surface pH approaches the pKa of this species. This behavior results in the observation of the secondary limiting current in lower pH values and explains why the second wave is not observed as clearly in the solutions with higher bulk pH. The comparison of the results from the present model with experimental cathodic polarization curves further confirmed this mechanistic view.

ACKNOWLEDGEMENTS

REFERENCES

1.   Zheng, Y., J. Ning, B. Brown, and S. Nesic, *Corrosion* 72 (2015): pp. 679–691.

2.   Zheng, Y., B. Brown, and S. Nešic, *Corrosion* 70 (2014): pp. 351–365.
3.   Bolmer, P.W., *Corrosion* 3 (1965): pp. 69–75.
4.   Esmaeely, S.N., B. Brown, and S. Nesic, *Corrosion* 73 (2017): pp. 144–154.
5.   Arzola, S., and J. Genescá, *J. Solid State Electrochem.* 9 (2005): pp. 197–200.
6.   Tribollet, B., J. Kittel, A. Meroufel, F. Ropital, F. Grosjean, and E.M.M. Sutter, *Electrochim. Acta* 124 (2014): pp. 46–51, http://dx.doi.org/10.1016/j.electacta.2013.08.133.
7.   Kittel, J., F. Ropital, F. Grosjean, E.M.M. Sutter, and B. Tribollet, *Corros. Sci.* 66 (2013): pp. 324–329, http://dx.doi.org/10.1016/j.corsci.2012.09.036.
8.   Esmaeely, S.N., G. Bota, B. Brown, and S. Nešić, *Corrosion* 74 (2018): pp. 37–49, http://corrosionjournal.org/doi/10.5006/2505.
9.   Gao, S., B. Brown, D. Young, and M. Singer, *Corros. Sci.* 165 (2018): pp. 171–179.
10.   Wen, X., P. Bai, B. Luo, S. Zheng, and C. Chen, *Corros. Sci.* 139 (2018): pp. 124–140, https://doi.org/10.1016/j.corsci.2018.05.002.
11.   Morris, D.R., *J. Electrochem. Soc.* 127 (1980): p. 1228.
12.   Shoesmith, D.W., *J. Electrochem. Soc.* 127 (1980): p. 1007.
13.   Galvan-Martinez, R., J. Mendoza-Flores, R. Duran-Romero, and J. Genesca, *Mater. Corros.* 58 (2007): pp. 514–521.
14.   Galvan-Martinez, R., J. Mendoza-Flores, R. Duran-Romero, and J. Genesca-Llongueras, *Mater. Corros.* 55 (2004): pp. 586–593.
15.   Arzola, S., J. Mendoza-Flores, R. Duran-Romero, and J. Genesca, *Corrosion* 62 (2006): pp. 433–443.
16.   Kahyarian, A., M. Singer, and S. Nesic, *J. Nat. Gas Sci. Eng.* 29 (2016): pp. 530–549, http://dx.doi.org/10.1016/j.jngse.2015.12.052.
17.   Zheng, Y., J. Ning, B. Brown, and S. Nesic, *Corros. 2014* 71 (2014): p. 316.
18.   Kahyarian, A., A. Schumaker, B. Brown, and S. Nesic, *Electrochim. Acta* 258 (2017): pp. 639–652.
19.   Kahyarian, A., M. Achour, and S. Nesic, "Mathematical Modeling of Uniform CO_2 Corrosion," in Trends Oil Gas Corros. Res. Technol., ed. A.M. El-Sherik (Elsevier, 2017), pp. 805–849.
20.   Marshall, W.L., and E.U. Franck, *J. Phys. Chem. Ref. Data* 10 (1983): pp. 295–304.
21.   Suleimenov, O.M., and R.E. Krupp, *Geochim. Cosmochim. Acta* 58 (1994): pp. 2433–2444.
22.   Suleimenov, O.M., and T.M. Seward, *Geochim. Cosmochim. Acta* 61 (1997): pp. 5187–5198.
23.   Migdisov, A.A., A.E. Williams-Jones, L.Z. Lakshtanov, and Y. V. Alekhin, *Geochim. Cosmochim. Acta* 66 (2002): pp. 1713–1725.
24.   Eigen, M., *Angew. Chem. Int. Ed. Engl.* 3 (1964): pp. 1–19.
25.   Eigen, M., *Angew. Chem. Int. Ed. Engl.* 3 (1964): pp. 1–72.
26.   Stillinger, F.H., *Theor. Chem. Adv.* 3 (1978): pp. 177–234.
27.   Tamimi, A., E.B. Rinker, and O.C. Sandall, *J. Chem. Eng. Data* 39 (1994): pp. 330–332.
28.   Haynes, W.M., ed., *CRC Handbook of Chemistry and Physics*, 84th ed. (CRC PRESS, 2004).
29.   Newman, J., and K.E. Thomas-Alyea, *Electrochemical Systems*, 3rd ed. (Wiley-interscience, 2004).
30.   Cochran, W.G., *Math. Proc. Cambridge Philos. Soc.* 1 (1934): pp. 365–375.
31.   Remita, E., B. Tribollet, E. Sutter, V. Vivier, F. Ropital, and J. Kittel, *Corros. Sci.* 50 (2008): pp. 1433–1440.
32.   Tran, T., B. Brown, and S. Nešic, *Corrosion* 70 (2014): pp. 223–229.
33.   Tran, T., B. Brown, S. Nesic, B. Tribollet, and S. Nešic, *Corros. 2013* 70 (2017): pp. 223–229.
34.   Eigen, M., and L. De Maeyer, *Proc. R. Soc. London, Ser. A* 247 (1958): pp. 505–533.
35.   Eigen, M., and E. Eyring, *J. Am. Chem. Soc.* 84 (1962): pp. 3254–3256.
36.   Eisenberg, M., C.W. Tobias, and C.R. Wilke, *J. Electrochem. Soc.* 101 (1954): pp. 306–320.